ACS OMEGA

Article

Cite This: ACS Omega 2019, 4, 9731−9738

http://pubs.acs.org/journal/acsodf

Difference in Electrochemical Mechanism of SnO_2 Conversion in Lithium-Ion and Sodium-Ion Batteries: Combined in Operando and Ex Situ XAS Investigations

Ditty Dixon,*[,†,∥] Marta Ávila,[‡] Helmut Ehrenberg,[†] and Aiswarya Bhaskar*[,†,§,∥]

[†]Karlsruhe Institute of Technology (KIT), Institute for Applied Materials (IAM), Hermann-von-Helmholtz-Platz 1, D-76344 Eggenstein-Leopoldshafen, Germany

[‡]ALBA Synchrotron, Carrer de la Llum, 2-26, Cerdanyola del Vallés, 08290 Barcelona, Spain

[§]Helmholtz Institute Ulm for Electrochemical Energy Storage (HIU), Albert-Einstein Allee 11, D-89081 Ulm, Germany

ABSTRACT: Conversion and alloying type negative electrodes attracted huge attention in the present research on lithium/sodium-ion batteries (LIBs/SIBs) due to the high capacity delivered. Among these, SnO_2 is investigated intensively in LIBs due to high cyclability, low reaction potential, cost-effectiveness, and environmental friendliness. Most of the LIB electrodes are explored in SIBs too due to expected similar electrochemical performance. Though several LIB negative electrode materials successfully worked in SIBs, bare SnO_2 shows very poor electrochemical performance in SIB. The reason for this difference is investigated here through combined *in operando* and *ex situ* X-ray absorption spectroscopy (XAS). For this, the electrodes of SnO_2 (space group $P4_2/mnm$ synthesized via one-pot hydrothermal method) were cycled in Na-ion and Li-ion half-cells. The Na/SnO_2 half-cell delivered a much lower discharge capacity than the Li/SnO_2 half-cell. In addition, higher irreversibility was observed for Na/SnO_2 half-cell during electrochemical investigations compared to that for Li/SnO_2 half-cell. *In operando* XAS investigations on the Na/SnO_2 half-cell confirms incomplete conversion and alloying reactions in the Na/SnO_2 half-cell, resulting in poor electrochemical performance. The difference in the lithiation and sodiation mechanisms of SnO_2 is discussed in detail.

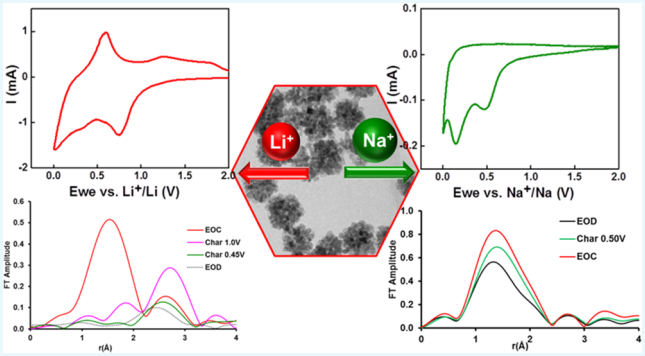

1. INTRODUCTION

While intercalation-type materials are intensively used as positive electrodes in lithium-ion batteries, the search for high-capacity negative electrodes focuses on conversion-type materials. Development of low-cost, high-capacity negative electrodes is highly essential to overcome the present safety concerns with the graphite negative electrode.[1,2] These materials include ternary and binary transition-metal oxides (MM'_2O_4, MO, M, and M′ = Fe, Co, Ni, Cu, etc.), phosphides, nitrides, intermetallic alloys, etc.[2−8] In addition to those, Sn-based materials have gained attention as negative electrode materials, particularly for lithium-ion batteries due to the reversible capacities exceeding 400 mAh g^{-1}.[9] Tin oxide, particularly SnO_2, has shown excellent electrochemical performance in Li-ion batteries.[10−17] Its capability as anode materials for Na-ion batteries is very promising due to the high capacity achievable (1378 mAh g^{-1}), where 711 mAh g^{-1} is obtained from a conversion reaction (involving $4Na^+$ ions per formula unit) and 667 mAh g^{-1} through an alloying reaction (by forming the Na-rich $Na_{15}Sn_4$ intermetallic).[18] Moreover, low average redox potential, environmentally benign nature, and comparatively low cost add to its advantages. However, the practical capacity for bare SnO_2 electrodes in Na-ion batteries is found to be much lower than the theoretical value, and the electrochemical reaction is found to be highly irreversible.[19,20] The reason behind this low practical capacity was attributed in some literature reports to the huge volume expansion of 520% occurring during the sodiation of Sn to $Na_{15}Sn_4$, which leads to pulverization and the resulting contact loss.[19] This irreversibility could not be overcome by modifying the morphology or reducing the particle size to below 100 nm.[19] The electrochemical reaction mechanism of SnO_2 in Na-ion batteries is proposed to be a conversion mechanism followed by alloying. Initially, SnO_2 by reacting with Na gets converted to Na_xSn, whose particles are embedded in a Na_2O matrix. Thereafter, with continuous increase in the concentration of Na in Na_xSn, the intermetallic phase $Na_{15}Sn_4$ will be crystallized.[20]

A combination of *in situ* transmission electron microscopy (TEM) and theoretical calculations using density functional theory has shown that the SnO_2 negative electrode can behave differently to lithiation and sodiation.[20] The diffusion of Na^+ in

Received: February 28, 2019
Accepted: May 10, 2019
Published: June 4, 2019

DOI: 10.1021/acsomega.9b00563
ACS Omega 2019, 4, 9731−9738

SnO_2 is calculated to be 30 times slower than that of Li^+. However, composite structures with carbon such as SnO_2−graphene nanocomposites with a three-dimensional architecture were found to deliver a capacity of >400 mAh g^{-1} over 200 cycles at a current density of 100 mA g^{-1} in Na-ion batteries.[21] Hence, it is important to note that the reported high capacities for SnO_2 in Na-ion batteries refer to a special material architecture containing different forms of carbon such as graphene or carbon nanotube and not just to bare SnO_2.[18,19,22,23]

Several investigations were conducted in literature to elucidate the electrochemical reaction mechanisms of SnO_2 in Li as well as Na half-cells.[20,22,24−27]

In 2013, Gu et al. probed the failure mechanism of SnO_2 with a nanowire morphology in Na-ion batteries using *in situ* TEM.[20] They observed that with sodiation, the SnO_2 nanowires undergo a structural change to Na_xSn, whose particles are dispersed in a matrix of Na_2O. This sodiation reaction is observed to induce a huge volume expansion (∼>100%).[20] Moreover, the sodiation speed was found to be ∼20 times lower than that of lithiation. In addition, the Sn particles surrounded by pores were formed as a result of desodiation due to the vacancies arising from dealloying of Na_xSn, which leads to a disconnected network, further resulting in the fading of the capacity of the SnO_2 nanowires after few cycles.[20] Ding et al. in 2014 reported a comparison of the phase-transformation mechanisms in Li/SnO_2 and Na/SnO_2 cells.[28] In the Na/SnO_2 cell, they observed the presence of unreacted β-Sn, surrounded by some amorphous material, which is assumed to be Na_xSn alloy at 0.01 V during discharge, that acts as an impediment. The slow kinetics of the reaction from Na−Sn alloys into intermetallic $Na_{15}Sn_4$ and the formation of intermediate crystalline SnO during Na_2O to SnO_2 conversion that blocks the Na^+ diffusion into metallic Sn are proposed as some of the reasons behind the low capacity obtained for the Na/SnO_2 cell.[28] Moreover, a systematic comparison of the sodiation- and lithiation-related phase changes reveals fundamental microstructural causes for the lower sodiation capacity than lithiation in SnO_2.[28] Different from the irreversible nature of sodiation, a fully reversible alloying and conversion reaction was observed for the Li/SnO_2 cell using X-ray diffraction (XRD).[28] However, the presence of some amount of amorphous residual material, that did not react back to the initial state after discharging, below the detection limit of the XRD cannot be ruled out at the end of the cycle.

In a work published by Górka et al. in 2015, the electrochemical reactions of SnO_2 thin films as well as SnO_2 mesoporous carbon composites with Li and Na were investigated and compared.[25] They observed a limited discharge capacity for the Na/SnO_2 system even with the use of 6−7 nm SnO_2 particles, which was attributed to a sluggish reaction kinetics due to the Na_2O matrix formed during the reaction. Even in the thin film, where the diffusion limitation is minimal, the amount of Na, which could be extracted during the 1st charge, was observed to be less than $1Na^+$ per SnO_2 and could be attributed to an intrinsic kinetic limitation of the sodiation reaction in the material.[25]

To further elucidate the reasons behind the limited Na storage capacity of bare SnO_2, *in operando* investigations were conducted on Na/SnO_2 half-cells using X-ray absorption spectroscopy (XAS) in this work. Though combined *ex situ* XRD, TEM, and XPS studies are reported already for the Na/SnO_2 system, only few *in operando* investigations were seen in the literature.[20,22,24,28,29] Moreover, *in operando* XAS, which can probe the bulk oxidation state changes is missing in the literature and is reported for the first time. In addition, Li/SnO_2 half-cells were also studied by XAS so that Li/SnO_2 and Na/SnO_2 can be compared. The investigated bare SnO_2 was synthesized through a one-pot hydrothermal route and is thoroughly characterized using X-ray diffraction, scanning electron microscopy (SEM), TEM, and electrochemical methods.

2. RESULTS AND DISCUSSION

Figure 1 displays the diffraction pattern of the as-synthesized SnO_2 sample. The set of reflections could be assigned to

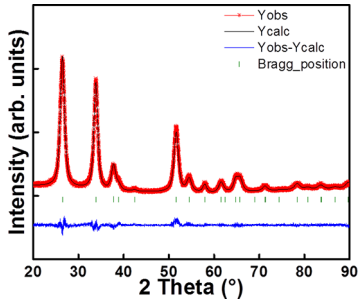

Figure 1. Rietveld refinement results based on X-ray diffraction data for the as-synthesized SnO_2.

tetragonal rutile SnO_2 with the space group $P4_2/mnm$. The obtained lattice parameters are $a = b = 4.7585(4)$ and $c = 3.1802(3)$ Å, respectively. The unit cell volume was found to be 72.014(4) $Å^3$. The volume-weighted average crystallite size in the a−b plane is about 6 nm and along the c-axis is about 8 nm. The lattice strain was calculated as 1.04×10^{-3}. No impurity phases were observed as revealed by the absence of additional reflections. In addition, the observed reflections were broader than the instrumental resolution function, indicating the nanocrystalline nature of the sample.

The SEM image of the as-synthesized SnO_2 sample is shown in Figure 2a. Primary particles 50−80 nm in diameter, with a sphere-like morphology, can be observed as agglomerated.

A closer look with TEM reveals that the material exists as flower-like secondary particles of ∼50 nm with primary particle size of ∼10 nm (see Figure 2b).

The cyclic voltammetry investigations were conducted at a scan rate of 0.1 mV s^{-1} in a voltage range 0.005−2.0 V vs Li^+/Li and vs Na^+/Na for Li/SnO_2 and Na/SnO_2 cells, respectively, and the results for the 1st and 5th cycles are displayed in Figure 3.

The shape of the cyclic voltammogram of the Li/SnO_2 half-cell is similar to the reports in literature.[14,30] The broad reduction peak observed at 0.75 V in the 1st cycle could be assigned to the crystal lattice destruction of the SnO_2 particles.[14] Another very broad reduction peak is observed at ∼0.30 V, which could be attributed to the alloying reaction of Sn with Li. A corresponding oxidation peak is visible at ∼0.6 V related to the Sn−Li dealloying reaction.[14,31] In addition, another set of broad reduction and oxidation peaks is observed at ∼0.57 and ∼1.26 V, which could be assigned to the SnO/Sn electrochemical reaction.[14] Moreover, in the 0.005−1.00 V discharging region of the CV, the broad peak also includes the formation of the solid−electrolyte interface layer.[18] The

DOI: 10.1021/acsomega.9b00563
ACS Omega 2019, 4, 9731−9738

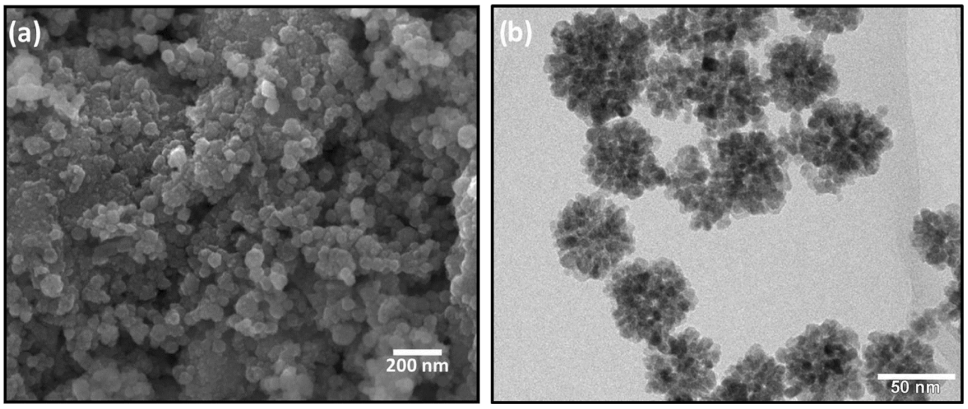

Figure 2. (a) Scanning electron microscopy (SEM) and (b) transmission electron microscopy (TEM) images of the as-synthesized SnO_2 by hydrothermal method.

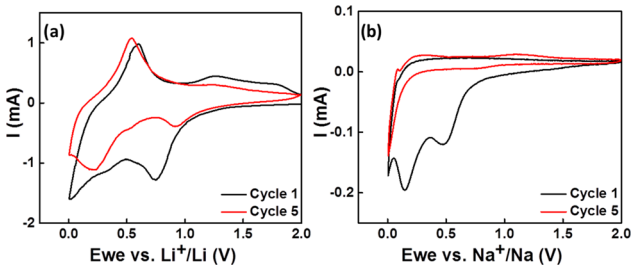

Figure 3. (a) Cyclic voltammograms of the 1st and 5th cycles of (b) Li/SnO_2 and Na/SnO_2 cells at a scan rate of 0.1 mV s^{-1} in a voltage range 0.005−2.000 V.

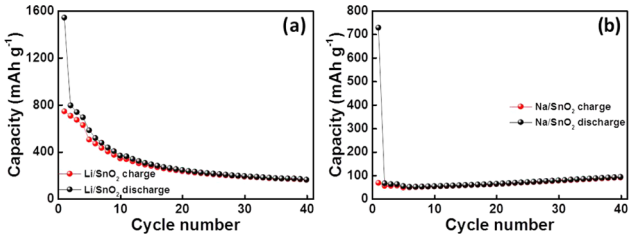

Figure 4. Cycle number vs capacity plots of (a) Li/SnO_2 and (b) Na/SnO_2 cells in the voltage range 0.005−2.000 V at 25 °C.

oxidation peak observed at ∼1.81 V could be attributed to the SnO_2/SnO reaction. Similar behavior was observed in the 5th cycle with slightly shifted voltages.[14]

For the Na/SnO_2 half-cell, the reduction peak starting around 1.6 V and coming down to lower voltages in the Na/SnO_2 half-cell could be attributed to the conversion reaction of SnO_2, probably without the completion of the alloying reaction as revealed by the low amount of capacity obtained in the charge−discharge experiment.[18] The broad peak observed around 0.4 V in the Na/SnO_2 half-cell corresponds to the formation of the solid−electrolyte interface.[18] In the anodic portion (oxidation part with positive currents) of the 1st cycle of the cyclic voltammogram as well as in the cathodic portion (reduction part with negative currents) of the 5th cycle of the cyclic voltammogram, only poorly defined peaks could be observed. In the anodic portion of the 5th cycle of the cyclic voltammogram, a small peak appears at ∼0.09 V, which is attributed in literature to the extraction of Na^+ from a carbon phase, which here could be the super C65 carbon used as a conductive additive.[18] In addition, broad peaks with very low charge flow were observed during the oxidation in the 5th cycle above ∼0. 25 V, which could be attributed to the dealloying reactions of Na−Sn alloys taking place at a very small extent. Overall, the very low charge flows demonstrate that only a low fraction of the active material is taking part in the electrochemical reaction; furthermore, the reaction remains incomplete at the end of the discharge/charge. These results are in agreement with the data shown in literature and indicate limited reversibility of conversion and alloying reactions of bare SnO_2 material in Na-ion batteries.[18,23]

The cyclic performances of the SnO_2 electrodes in Li and Na half-cells are displayed in Figure 4a,b, respectively. The measurements were conducted at a charge−discharge rate of C/10 for the initial four cycles and C/5 for the subsequent cycles in a voltage range 0.005−2.00 V for Li/SnO_2. For the Na/SnO_2 cell, slower charge−discharge rates were applied for the cycling experiments due to the sluggish diffusion of Na^+ ions in comparison with that of Li^+ ions. Hence, the charge−discharge rate of C/20 was applied for the initial four cycles followed by a C-rate of C/10 for the subsequent cycles in the voltage range 0.005−2.00 V.

The number of electrons flowing through the outer circuit during the first discharge for the Li/SnO_2 half-cell correspond to a capacity of 1542 mAh g^{-1}. In the successive charge, the Li/SnO_2 cell delivered a capacity of 744 mAh g^{-1}, which is close to the theoretical capacity (781 mAh g^{-1}), displaying a Coulombic efficiency of only 48%. This behavior is already well known for the SnO_2 material, and the lower Coulombic efficiency is attributed to the formation of solid electrolyte interface (SEI) as well as to the irreversible amorphous lithium oxide on the surface of the electrode.[30,32] The Coulombic efficiency increases after the 1st cycle and reaches a value of ∼98% after several cycles. The material exhibited a capacity retention of ∼20% after 40 cycles, which is close to that of the values reported in literature for bare, non-modified SnO_2 samples in the Li half-cells.[11,13]

In the Na half-cells, the SnO_2 electrode delivers an initial discharge capacity of 728 mAh g^{-1}. In the successive charge, the Na/SnO_2 cell delivered a capacity of only 67 mAh g^{-1}, which is much lower than the theoretical capacity (781 mAh g^{-1}), and this behavior is in agreement with the literature data.[13,19] The Coulombic efficiency of the Na/SnO_2 cell in the 1st cycle was as low as 9%. This lower Coulombic efficiency could be attributed to the formation of a solid electrolyte interface (SEI) as well as to any irreversibility in the electrochemical reaction. Moreover, it was interesting to

DOI: 10.1021/acsomega.9b00563
ACS Omega 2019, 4, 9731−9738

observe that the absolute capacity values of the Na/SnO_2 cell gradually increases after few initial cycles. A similar behavior was observed in literature reports for the SnO_2 composite electrodes when cycled against Li and Na and for amorphous carbon when cycled against Li or Na.[18,19,22] This could be due to some conditioning of the electrode materials with respect to the structure or SEI during cycling or due to the involvement of carbon in the electrochemical reaction, and this requires further investigation. The Na/SnO_2 cell delivered charge and discharge capacities of 90 and 92 mAh g^{-1}, respectively, after 40 cycles. The charge capacity delivered was ~34% in excess compared to the initial value.

2.1. *In Operando* and *Ex Situ* XAS Investigations. The charge−discharge voltage profiles of the Li/SnO_2 half-cell (C-rate C/15) are displayed in Figure 5a, where the selected

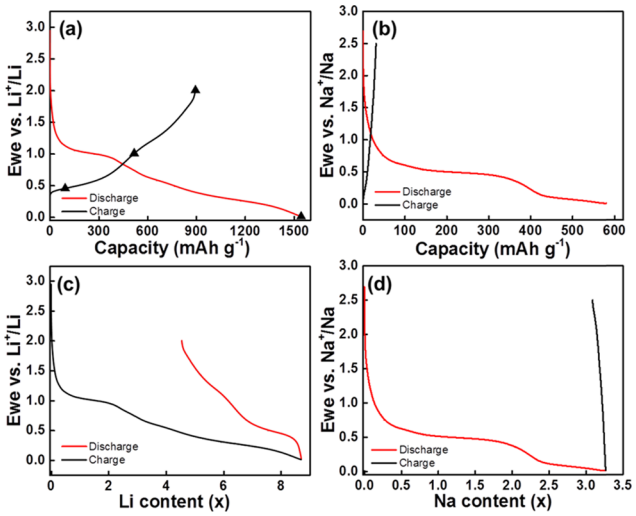

Figure 5. First charge−discharge voltage profiles of (a) Li/SnO_2 cell and (b) Na/SnO_2 cell used for the XAS investigations. Plots of (c) voltage vs Li content in Li/SnO_2 cell and (d) voltage vs Na content in Na/SnO_2 cell used for the XAS investigations. The voltages at which *ex situ* samples were prepared for Li/SnO_2 cell are marked with "▲". The voltage range applied for conducting the experiment was 0.005−2.000 V for the Li/SnO_2 cell and 0.005−2.50 V for the Na/SnO_2 cell.

voltages for the preparation of the *ex situ* samples are marked. The corresponding lithiation states are shown in Figure 5c. The charge−discharge voltage profiles of the 1st cycle conducted for Na/SnO_2 (charge rate C/40 and discharge rate C/30) during *in operando* XAS measurements are displayed in Figure 5b.

While a discharge capacity of 1549 mAh g^{-1} was delivered by the Li/SnO_2 half-cell, only 580 mAh g^{-1} was delivered by the Na/SnO_2 half-cell. Correspondingly, 8.71 mol of Li and 3.26 mol of Na participated in the electrochemical reaction during the discharge of the SnO_2 electrode in Li half-cell and Na half-cell, respectively, as calculated from the electron flow through the circuit (see Figure 5c,d). Note that in the case of Li/SnO_2 half-cell, the number of moles of Li inserted into the SnO_2 electrode is almost twice the theoretical amount of Li able to be incorporated. This is a usual phenomenon reported in literature and is attributed to the additional alloying reaction as well as to side reactions with electrolyte.[30,32,33] Moreover, at the end of the cycle, the Li/SnO_2 cell regained a capacity of 898 mAh g^{-1}, whereas the Na/SnO_2 cell could deliver a capacity of 31 mAh g^{-1} only, even when the upper cutoff voltage was extended to 2.5 V. The corresponding Coulombic efficiencies are 58 and 5.3% for the Li/SnO_2 and Na/SnO_2 cells, respectively, and the corresponding number of moles of Li and Na involved in the charge are 4.2 and 0.17 mol per 1 mol of SnO_2, respectively.

2.1.1. Li/SnO_2 Half-Cell. To elucidate the electrochemical mechanism of Li insertion in SnO_2, corresponding *in operando* XAS spectra on the Sn K edge were analyzed. During the 1st discharge, where the first Li^+ uptake takes place, the position of the Sn K edge shifted to a lower energy, indicating a reduction of Sn^{4+} to Sn^0 oxidation state. At the discharge voltage of around 0.35 V, the edge position almost overlapped with that of the metallic Sn foil spectra, indicating a complete conversion of SnO_2 to metallic Sn. However, towards the end of discharge, the edge position shifted again to higher energy. At this voltage of 0.005 V, a reoxidation of Sn can be ruled out. Therefore, this shift to higher energy at the end of discharge corresponds to the alloying of Li and Sn.[33] Furthermore, it can also be observed that the white line intensity of the Sn K edge continuously decreases during discharging. This indicates changes in the average local coordination corresponding to an increase in the coordination of Sn−Sn and a decrease in the coordination of Sn−O (see Figure 6a).[27]

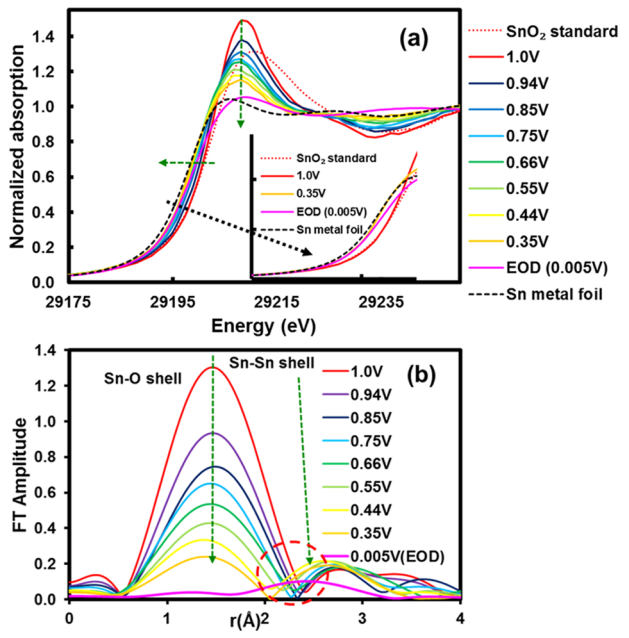

Figure 6. (a) Sn K edge X-ray absorption near edge structure (XANES) spectra during discharging of Li/SnO_2 cell and the (b) corresponding extended X-ray absorption fine structure (EXAFS) Fourier transform (FT). Inset: magnified Sn K edge region.

Direct information about the local coordination can be obtained from the EXAFS Fourier transform (FT). The EXAFS FT of the fresh sample is characterized by a peak between 1 and 2 Å corresponding to the Sn−O shell. The amplitude of this peak decreases continuously during discharge while a new peak evolves around 2−3 Å, characteristic for metallic Sn (Sn−Sn shell). At 0.35 V, the amplitude of this peak reached its maximum. Upon further discharge, the amplitude of this peak decreased. This behavior greatly differs from the conversion anodes based on oxides of first-row transition metals by the fact that any decrease in the intensity of metal/oxygen shell is usually accompanied by an increase in

DOI: 10.1021/acsomega.9b00563
ACS Omega 2019, 4, 9731−9738

the metal/metal shell.[34] This different behavior observed for the SnO_2 system can be explained by the Li alloying mechanism. During the alloying, Li enters into the Sn metal lattice, which gives a different EXAFS signal. A similar behavior was also observed for the Pt/Ru alloy nanoparticle system.[35] During the charging cycle, it was observed that the FT amplitude of the Sn−Sn shell increased and reached a maximum around 1.0 V (Figure 7a).

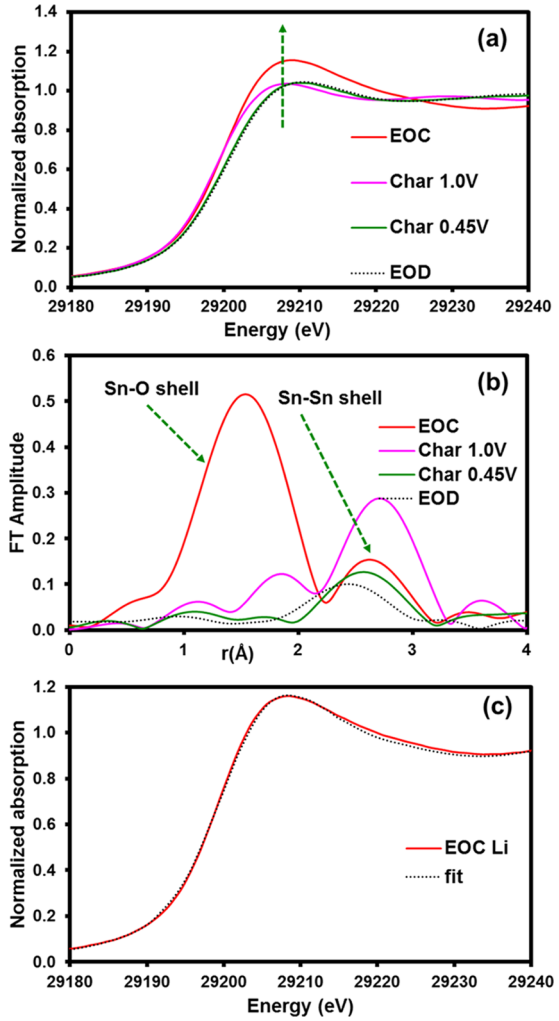

Figure 7. (a) Sn K edge XANES spectra during charging of Li/SnO_2 cell, (b) corresponding EXAFS FT, and (c) linear combination fitting (LCF) analysis of the end-of-charge (EOC) sample with Sn foil, SnO_2, and $SnCl_2$ spectra as references.

The increase in the FT amplitude could be attributed to the removal of Li from the Li−Sn alloy (dealloying), which is just the opposite behavior seen during the discharge cycle. Upon further charging, a prominent peak corresponding to the Sn−O shell was formed between 1 and 2 Å. This is further reflected in the XANES region, where the edge position was also shifted to higher energy during charging. In the fully charged state or at the end of charge (EOC), the white line intensity and the energy of the absorption edge reached a maximum value. Nevertheless, when compared to the fresh sample, the cycled sample showed a reduced white line intensity as well as a lower energy for the absorption edge. Similarly, in the EXAFS FT, the Sn−O shell of the cycled sample was also characterized by a lower amplitude compared to the fresh sample. Moreover, a significant Sn−Sn shell was still visible for the cycled sample. Thus, it may be concluded that the conversion of metallic Sn back to SnO_2 is only partial. Residual metallic fractions are seen at the end of charge for several conversion anodes, and this phenomenon is one of the main reasons behind the capacity fade observed for those systems.[34]

However, the metallic Sn fraction seen for the SnO_2 system may not contribute as much to the overall capacity fade of Li/SnO_2 cells in comparison with other conversion oxide systems, as there is a possibility for this Sn fraction to alloy with Li in the subsequent cycles.[27] Linear combination fitting (LCF) analysis of the cycled sample spectra with Sn metal foil, $SnCl_2$, and SnO_2 reference compounds confirmed the presence of 28% metallic Sn phase in the fully cycled state (Figure 7c). Moreover, the oxide phase formed at the end of the cycling was characterized by contributions of Sn^{2+} and Sn^{4+} species in a ratio 1:1. Please note that LCF analysis was not done on the EOD sample with Li, as no reference spectra were found suitable for quantifying the Sn−Li intermetallics, which are present at the intermediate states of discharge.

2.1.2. Na/SnO_2 Half-Cell. The XANES region of the XAS spectra obtained during the electrochemical discharging of SnO_2 with Na showed almost similar behavior compared to the discharging with Li. Nevertheless, the decrease in the white line intensity observed during the discharge of SnO_2 with Na was less pronounced than in the Li case. The edge position continuously shifted to lower energy for the lower half-cell voltage. Note that the shift of the XANES spectra to higher energies, as observed during the EOD of SnO_2 with Li, was not observed at the EOD with Na. Moreover, the XANES spectra obtained at the lower voltage with Na during discharge never showed a full metallic character. Therefore, complete conversion of SnO_2 to its metallic or alloy state can be ruled out. This conclusion is further supported by the EXAFS FT, as a prominent peak corresponding to the Sn−O shell was still present at the EOD with Na (Figure 8a,b). The linear combination fitting analysis of the EOD XAS spectrum of the Na/SnO_2 cell showed a contribution of 42, 33, and 25% contribution from Sn^{4+}, Sn^{2+}, and Sn^0 species, respectively (Figure 8c).

One of the reasons for this poor electrochemical behavior for the Na/SnO_2 half-cell in comparison with the Li/SnO_2 half-cell might be the denser Na_2O shell, which acts as an ionic as well as electronic insulator and prevents further reduction of SnO_2. This is reflected by 42% inactive SnO_2 in the Na/SnO_2 cell at the EOD. The LCF analysis indicated 25% of Sn in the metallic state at the EOD. However, a corresponding Sn−Sn shell was not visible in the EXAFS FT. During alloying, Na enters into the Sn metal lattice, which gives rise to a destructive interference of the signal arising from the Sn−Sn metallic shell. Such a behavior was also observed for other alloy nanoparticle systems. Hence, the absence of peak corresponding to the Sn−Sn shell besides the presence of 25% of metallic Sn could indicate the Na−Sn alloy formation.[35,36] Finally, during Na extraction in the following charging, the XANES spectra were characterized by a slight increase in the white line intensity as well as a small shift to higher energy when compared with the EOD state. This is further reflected in the EXAFS FT as the amplitude of the Sn−O shell showed only a slight increase (Figure 9a,b).

The LCF analysis showed that 63% Sn^{4+} and 37% Sn^{2+} species contributed to the spectra of the EOC state (Figure 9c). Thus, all metallic fraction formed during the discharging

DOI: 10.1021/acsomega.9b00563
ACS Omega 2019, 4, 9731−9738

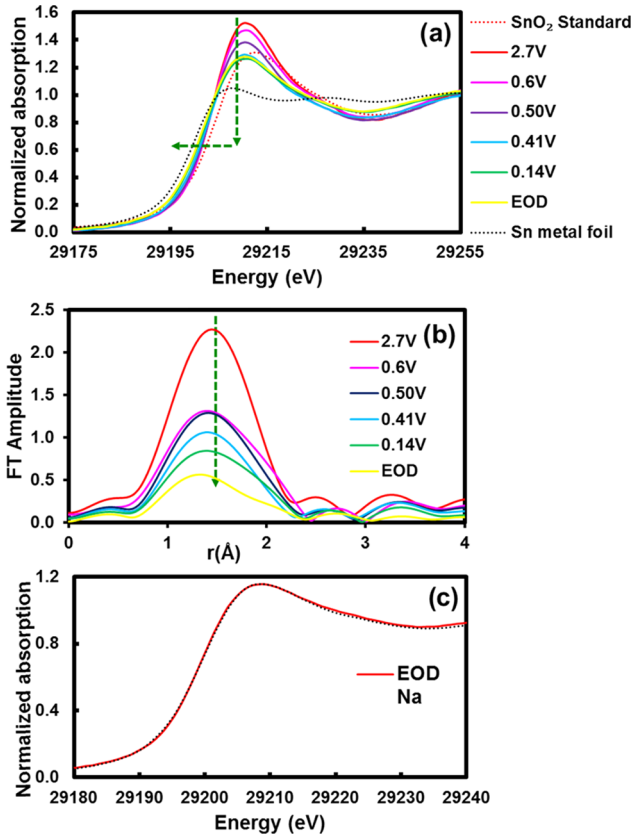

Figure 8. (a) Sn K edge XANES spectra during discharging of Na/SnO_2 cell, (b) the corresponding EXAFS FT, and (c) LCF analysis of the EOD sample with Sn foil, SnO_2, and $SnCl_2$ spectra as references.

(Na uptake) is completely reoxidized. The absence of any metallic Sn after cycling can be explained based on a core–shell model: the small fraction of metallic phase, formed during discharge, builds a shell around a core with unreacted SnO_2 embedded in a thick layer of Na_2O. Therefore, it may be concluded that SnO_2 does not achieve a complete and uniform conversion/alloying reaction with Na because of the formation of a dense Na_2O layer, which blocks electronic and ionic transport into the inner region of the SnO_2 particles, in contrast to the reaction with Li.

3. CONCLUSIONS

Phase-pure SnO_2 nanoparticles with flower-like morphology were synthesized by a one-pot hydrothermal route. The synthesized SnO_2 nanoparticles were cycled in half-cells against Li as well as Na. Compared to the Li/SnO_2 half-cell, the Na/SnO_2 half-cell delivered a much lower absolute reversible capacity. The reasons for this electrochemical performance difference were elucidated using *in operando* as well as *ex situ* XAS investigations using an in-house-designed electrochemical test cell. The *in operando* Sn K edge XAS studies revealed a significant difference between the lithiation and sodiation processes in SnO_2. The lithiation of SnO_2 was associated with the complete reduction of SnO_2 to metallic Sn and successive alloying of Li with Sn. The subsequent charging process starts by dealloying Li, followed by conversion back to tin oxide. However, the presence of a small amount of metallic Sn was still observed at the end of the first cycle. As far as the sodiation on SnO_2 is concerned, discharging with Na is associated with incomplete conversion of SnO_2 to metallic Sn.

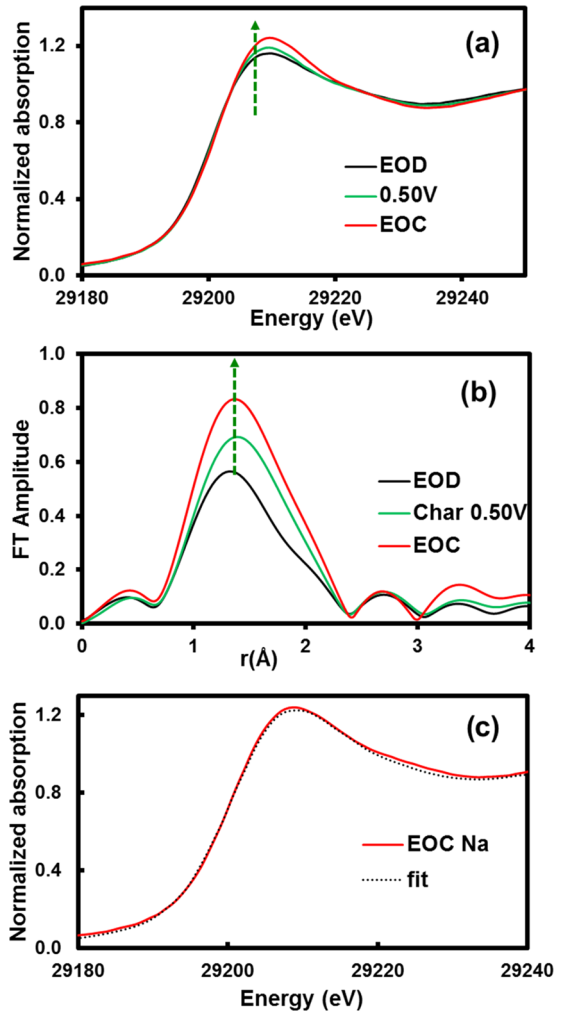

Figure 9. (a) Sn K edge XANES spectra during charging of Na/SnO_2 cell, (b) the corresponding EXAFS FT, and (c) LCF analysis of the EOC sample with Sn foil, SnO_2, and $SnCl_2$ spectra as references.

This incomplete conversion of SnO_2 can be attributed to the formation of a dense Na_2O layer, which acts as a transport barrier to the flow of Na^+ ions and electrons.

4. EXPERIMENTAL SECTION

4.1. Synthesis. The SnO_2 samples were synthesized using a one-pot hydrothermal method similar to the synthesis described elsewhere.[10] For this, the sodium stannate, $Na_2SnO_3{\cdot}3H_2O$ (Sigma-Aldrich) precursor was dissolved in ethanol–water mixed solvent. The mixture was then heated in a Teflon-lined stainless steel autoclave of 100 mL capacity at 180 °C for 24 h. The obtained suspension was centrifuged and dried to separate the final SnO_2 sample.

4.2. Structural Characterization. Powder X-ray diffraction (XRD) pattern of the as-synthesized SnO_2 sample was recorded using a STOE Stadi P powder diffractometer, equipped with a Dectris Mythen 1 K Silicon strip detector, a focusing Ge(111) monochromator (Cu $K_{\alpha 1}$ radiation; λ = 1.540562 Å), and a step width of 0.015° (2θ), in a flat-sample transmission mode. Rietveld refinement was applied for data analysis using the WinplotR package.[37] For all the refined parameters, the standard deviations were calculated in agreement with Bérar and Lelann.[38]

DOI: 10.1021/acsomega.9b00563
ACS Omega 2019, 4, 9731–9738

4.3. Morphology and Particle Size Characterization. The morphology of the as-synthesized SnO_2 powder was analyzed using a Zeiss Supra 55 Scanning Electron Microscope with primary energies of 5 and 15 keV and an in-lens detector. The particle sizes were analyzed by transmission electron microscopy using a Philips CM20 TEM with an acceleration voltage of 200 kV and LaB_6 cathode.

4.4. Electrochemical Characterization. To prepare the SnO_2 electrodes, 70% (w/w) active material, 20% (w/w) super C65 carbon (TIMCAL) as conductive additive, and 10% (w/w) poly(vinylidenefluoride) (Solef PVdF 6020 binder, Solvay) were mixed in *N*-methyl-2-pyrrolidone (NMP, Sigma-Aldrich). The obtained slurry was then coated on a Cu foil with a wet thickness of 300 μm. The coated foil was then dried overnight at 80 °C. Electrode disks 1.2 cm in diameter were punched out of the foil, followed by overnight vacuum drying at 110 °C. The mass loadings of the obtained electrodes were ∼2−3 mg. To conduct the electrochemical experiments, two-electrode Swagelok-type test cells were assembled in an argon-filled glovebox with SnO_2 as the working electrode. For the Li half-cells, lithium foil (Alfa Aesar) was used as the counter and reference electrodes, glass microfiber filters (Whatmann-GF/D 70 mm Ø) were used as the separator, and LP30 (1 M $LiPF_6$ in ethylenecarbonate:dimethylcarbonate = 1:1) as the electrolyte. For the Na half-cells, metallic Na was used as the counter and reference electrodes, glass microfiber filters (Whatmann-GF/D 70 mm Ø) were used as the separator, and 1 M $NaClO_4$ in propylenecarbonate as the electrolyte. All electrodes were electrochemically characterized with a VMP3 multichannel potentiostat (Bio-Logic, France) at 25°C for the *ex situ* experiments and at ambient temperature for the *in operando* experiments. For the *ex situ* XAS experiments, the prepared cells were galvanostatically charged and discharged to different cutoff voltages. Note that "charge" here refers to delithiation/desodiation, and discharge refers to lithiation/sodiation, respectively, in the Li/SnO_2 and Na/SnO_2 half-cells. Moreover, 1C is defined as 782 mA g^{-1}. The charged or discharged cells were then transferred to a glovebox with Ar atmosphere and O_2 and H_2O concentrations below 1 ppm. The cells were disassembled, and the SnO_2 electrodes with different states of charge or discharge were taken out. These electrodes were then glued between Kapton tapes. A pristine electrode was used for comparison.

4.5. *In Operando* and *Ex Situ*XAS Investigations. The electrochemical mechanisms of Li/SnO_2 and Na/SnO_2 cells were investigated using *in operando* and *ex situ*X-ray absorption spectroscopy (XAS) at the Sn K edge. For the *in operando* experiments, cells similar to those reported in a previous work were used.[34,39] The prepared cell was placed in a sample holder and aligned. The *in operando* XAS spectra of the Li/SnO_2 cell were recorded at the Sn K edge at beamline BM 23, ESRF, and Grenoble in fluorescence geometry, and Si(311) monochromatized beam was used to record the Sn K edge spectra. Only the 1st discharge until 0.35 V was studied for the Li/SnO_2 cell with the *in operando* technique due to limited beamtime. *In operando* XAS spectra during a complete cycle of Na/SnO_2 cell and the *ex situ* XAS spectra of the disassembled electrodes for Li half-cells including the end of discharge (EOD) of the 1st cycle were recorded in transmission geometry at CLAESS, ALBA Synchrotron, Barcelona. Si(311) monochromatized beam was used to record the Sn K edge spectra. The details of the cell used and the measurement technique are published elsewhere.[34,39] Processing of the spectra was performed using the Demeter software package.[40]

AUTHOR INFORMATION

Corresponding Authors

*E-mail: ditty@cecri.res.in (D.D.).
*E-mail: aiswarya@cecri.res.in (A.B.).

ORCID

Helmut Ehrenberg: 0000-0002-5134-7130
Aiswarya Bhaskar: 0000-0003-0557-5199

Present Address

‖Electrochemical Power Sources Division, CSIR-CECRI, Karaikudi 630003, Tamil Nadu, India (D.D.) (A.B.).

Author Contributions

The manuscript was written through contributions of all authors. All authors have given approval to the final version of the manuscript. The authors declare no competing financial interest.

Notes

The authors declare no competing financial interest.

ACKNOWLEDGMENTS

This work contributes to the research performed at CELEST (Center for Electrochemical Energy Storage Ulm-Karlsruhe) and is funded by the Deutsche Forschungsgemeinschaft (DFG, German Research Foundation) under Germany's Excellence Strategy, EXC-2154/1, Project A.3.1. This work has further benefited from beam time allocation by the core-level absorption and emission spectroscopies (CLAESS) beamline at ALBA in Barcelona and at BM 23 beamline from ESRF in Grenoble. Gleb Parakhonskiy and Olivier Mathon from ESRF, Grenoble, are thankfully acknowledged for their technical support. Department of Materials and Earth Sciences affiliated to TU Darmstadt is gratefully acknowledged for providing the TEM facility. Bettina Hunzinger is gratefully acknowledged for the technical support with SEM.

REFERENCES

(1) Liu, K.; Liu, Y.; Lin, D.; Pei, A.; Cui, Y. Materials for Lithium-Ion Battery Safety. *Sci. Adv.* **2018**, *4*, No. eaas9820.
(2) Cabana, J.; Monconduit, L.; Larcher, D.; Palacín, M. R. Beyond Intercalation-Based Li-Ion Batteries: The State of the Art and Challenges of Electrode Materials Reacting through Conversion Reactions. *Adv. Mater.* **2010**, *22*, E170−E192.
(3) DeMattei, R. C.; Watcharapasorn, A.; Feigelson, R. S. Conditions for the Electrochemical Synthesis of the $CoPn_3$ (Pn = P, As, Sb) Skutterudites. *J. Electrochem. Soc.* **2001**, *148*, D109−D111.
(4) Poizot, P.; Laruelle, S.; Grugeon, S.; Dupont, L.; Tarascon, J. Nano-Sizedtransition-Metaloxidesas Negative-Electrode Materials for Lithium-Ion Batteries. *Nature* **2000**, *407*, 496−499.
(5) Chen, C.; Ding, N.; Wang, L.; Yu, Y.; Lieberwirth, I. Some New Facts on Electrochemical Reaction Mechanism for Transition Metal Oxide Electrodes. *J. Power Sources* **2009**, *189*, 552−556.
(6) Wadewitz, D.; Gruner, W.; Herklotz, M.; Klose, M.; Giebeler, L.; Voss, A.; Thomas, J.; Gemming, T.; Eckert, J.; Ehrenberg, H. Investigation of Copper-Cobalt-Oxides as Model Systems for Composite Interactions in Conversion-Type Electrodes for Lithium-Ion Batteries. *J. Electrochem. Soc.* **2013**, *160*, A1333−A1339.
(7) Adam, R.; Wadewitz, D.; Gruner, W.; Klemm, V.; Ehrenberg, H.; Rafaja, D. Phase and Microstructure Development in the Conversion Type Electrodes for Li-Ion Batteries Based on the Cu-Fe-O System. *J. Electrochem. Soc.* **2013**, *160*, A1594−A1603.

DOI: 10.1021/acsomega.9b00563
ACS Omega 2019, 4, 9731−9738

(8) Nitta, N.; Yushin, G. High-Capacity Anode Materials for Lithium-Ion Batteries: Choice of Elements and Structures for Active Particles. *Part. Part. Syst. Charact.* **2014**, *31*, 317−336.
(9) Liu, L.; Xie, F.; Lyu, J.; Zhao, T.; Li, T.; Gill, B. Tin-Based Anode Materials with Well-Designed Architectures for Next-Generation Lithium-Ion Batteries. *J. Power Sources* **2016**, *321*, 11−35.
(10) Lou, X. W.; Wang, Y.; Yuan, C.; Lee, J. Y.; Archer, L. A. Template-Free Synthesis of SnO_2 Hollow Nanostructures with High Lithium Storage Capacity. *Adv. Mater.* **2006**, *18*, 2325−2329.
(11) Wang, D.; Li, X.; Wang, J.; Yang, J.; Geng, D.; Li, R.; Cai, M.; Sham, T. K.; Sun, X. Defect-Rich Crystalline SnO_2 Immobilized on Graphene Nanosheets with Enhanced Cycle Performance for Li-Ion Batteries. *J. Phys. Chem. C* **2012**, *116*, 22149−22156.
(12) Guo, Q.; Zheng, Z.; Gao, H.; Ma, J.; Qin, X. SnO_2/graphene Composite as Highly Reversible Anode Materials for Lithium Ion Batteries. *J. Power Sources* **2013**, *240*, 149−154.
(13) Guo, Q.; Qin, X. Flower-like SnO_2 Nanoparticles Grown on Graphene as Anode Materials for Lithium-Ion Batteries. *J. Solid State Electrochem.* **2014**, *18*, 1031−1039.
(14) Reddy, M. V.; Andreea, L. Y. T.; Ling, A. Y.; Hwee, J. N. C.; Lin, C. A.; Admas, S.; Loh, K. P.; Mathe, M. K.; Ozoemena, K. I.; Chowdari, B. V. R. Effect of Preparation Temperature and Cycling Voltage Range on Molten Salt Method Prepared SnO_2. *Electrochim. Acta* **2013**, *106*, 143−148.
(15) Zhou, X.; Huang, B.; Zou, Y.; Xie, J.; Yang, J. Cotton-Templated Fabrication of Hierarchical SnO_2 Mesoporous Microtubes as the Anode Material of Lithium Ion Battery. *Mater. Lett.* **2014**, *120*, 279−282.
(16) Yang, T.; Lu, B. Highly Porous Structure Strategy to Improve the SnO_2 Electrode Performance for Lithium-Ion Batteries. *Phys. Chem. Chem. Phys.* **2014**, *16*, 4115−4121.
(17) Liu, X.; Zhang, J.; Si, W.; Xi, L.; Oswald, S.; Yan, C.; Schmidt, O. G. High-Rate Amorphous SnO_2 Nanomembrane Anodes for Li-Ion Batteries with a Long Cycling Life. *Nanoscale* **2015**, *7*, 282−288.
(18) Ding, J.; Li, Z.; Wang, H.; Cui, K.; Kohandehghan, A.; Tan, X.; Karpuzov, D.; Mitlin, D. Sodiation vs Lithiation Phase Transformations in a High Rate − High Stability SnO_2 in Carbon Nanocomposite. *J. Mater. Chem. A* **2015**, *3*, 7100−7111.
(19) Jahel, A.; Ghimbeu, C. M.; Darwiche, A.; Vidal, L.; Hajjar, S.; Vix-Guterl, C.; Monconduit, L. Exceptionally Highly Performing Na-Ion Battery Anode Using Crystalline SnO_2 Nanoparticles Confined in Mesoporous Carbon. *J. Mater. Chem. A* **2015**, *3*, 11960−11969.
(20) Gu, M.; Kushima, A.; Shao, Y.; Zhang, J.; Liu, J.; Browning, N. D.; Li, J.; Wang, C. Probing the Failure Mechanism of SnO_2 Nanowires for Sodium-Ion Batteries. *Nano Lett.* **2013**, *13*, 5203−5211.
(21) Pei, L.; Jin, Q.; Zhu, Z.; Zhao, Q.; Liang, J.; Chen, J. Ice-Templated Preparation and Sodium Storage of Ultrasmall SnO_2 Nanoparticles Embedded in Three-Dimensional Graphene. *Nano Res.* **2015**, *8*, 184−192.
(22) Lu, Y. C.; Ma, C.; Alvarado, J.; Kidera, T.; Dimov, N.; Shirley, Y.; Okada, S. Electrochemical Properties of Tin Oxide Anodes for Sodium-Ion Batteries. *J. Power Sources* **2015**, *284*, 287−295.
(23) Zhao, X.; Zhang, Z.; Yang, F.; Fu, Y.; Lai, Y.; Li, J. Core-Shell Structured SnO_2 Hollow Spheres-Polyaniline Composites as Anode for Sodium-Ion Batteries. *RSC Adv.* **2015**, *5*, 31465−31471.
(24) Li, Z.; Ding, J.; Mitlin, D. Tin and Tin Compounds for Sodium Ion Battery Anodes: Phase Transformations and Performance. *Acc. Chem. Res.* **2015**, *48*, 1657−1665.
(25) Górka, J.; Baggetto, L.; Keum, J. K.; Mahurin, S. M.; Mayes, R. T.; Dai, S.; Veith, G. M. The Electrochemical Reactions of SnO_2 with Li and Na: A Study Using Thin Films and Mesoporous Carbons. *J. Power Sources* **2015**, *284*, 1−9.
(26) Huang, J. Y.; Zhong, L.; Wang, C. M.; Sullivan, J. P.; Xu, W.; Zhang, L. Q.; Mao, S. X.; Hudak, N. S.; Liu, X. H.; Subramanian, A.; et al. In Situ Observation of the Electrochemical Lithiation of a Single SnO_2 Nanowire Electrode. *Science* **2010**, *330*, 1515−1521.
(27) Pelliccione, C. J.; Timofeeva, E. V.; Segre, C. U. Potential-Resolved *In Situ* X-Ray Absorption Spectroscopy Study of Sn and SnO_2 Nanomaterial Anodes for Lithium-Ion Batteries. *J. Phys. Chem. C* **2016**, *120*, 5331−5339.
(28) Ding, J.; Li, Z.; Wang, H.; Cui, K.; Kohandehghan, A.; Tan, X.; Karpuzov, D.; Mitlin, D. Sodiation vs. Lithiation Phase Transformations in a High Rate − High Stability SnO_2 in Carbon Nanocomposite. *J. Mater. Chem. A* **2015**, *3*, 7100−7111.
(29) Bhaskar, A.; Dixon, D.; Avila, M.; Balachandran, G.; Bramnik, N.; Ehrenberg, H. In *Difference in the Electrochemical Mechanism of SnO_2 in Lithium-Ion and Sodium-Ion Batteries: An in Situ XAS Study*, ECS Meeting Abstracts, 2016; pp MA2016−03866.
(30) Kuriganova, A. B.; Vlaic, C. A.; Ivanov, S.; Leontyeva, D. V.; Bund, A.; Smirnova, N. V. Electrochemical Dispersion Method for the Synthesis of SnO_2 as Anode Material for Lithium Ion Batteries. *J. Appl. Electrochem.* **2016**, *46*, 527−538.
(31) Reddy, M. V.; Tse, L. Y.; Bruce, W. K. Z.; Chowdari, B. V. R. Low Temperature Molten Salt Preparation of Nano-SnO_2 as Anode for Lithium-Ion Batteries. *Mater. Lett.* **2015**, *138*, 231−234.
(32) Ye, F.; Zhao, B.; Ran, R.; Shao, Z. Facile Mechanochemical Synthesis of Nano SnO_2/ Graphene Composite from Coarse Metallic Sn and Graphite Oxide: An Outstanding Anode Material for Lithium-Ion Batteries. *Chem. - Eur. J.* **2014**, *20*, 4055−4063.
(33) Kim, H.; Park, G. O.; Kim, Y.; Muhammad, S.; Yoo, J.; Balasubramanian, M.; Cho, Y.; Kim, M.; Lee, B.; Kang, K.; et al. New Insight into the Reaction Mechanism for Exceptional Capacity of Ordered Mesoporous SnO_2 Electrodes via Synchrotron-Based X-Ray Analysis. *Chem. Mater.* **2014**, *26*, 6361−6370.
(34) Balachandran, G.; Dixon, D.; Bramnik, N.; Bhaskar, A.; Yavuz, M.; Pfaffmann, L.; Scheiba, F.; Mangold, S.; Ehrenberg, H. Elucidation of the Electrochemical Reaction Mechanism in MFe_2O_4 (M = Ni, Co) Conversion-Type Negative Electrode Systems by Using *In Situ* X-Ray Absorption Spectroscopy. *Chemelectrochem* **2015**, *2*, 1510−1518.
(35) Dixon, D.; Wippermann, K.; Mergel, J.; Schoekel, A.; Zils, S.; Roth, C. Degradation Effects at the Methanol Inlet, Outlet and Center Region of a Stack MEA Operated in DMFC. *J. Power Sources* **2011**, *196*, 5538−5545.
(36) Russell, A. E.; Rose, A. X-Ray Absorption Spectroscopy of Low Temperature Fuel Cell Catalysts. *Chem. Rev.* **2004**, *104*, 4613−4635.
(37) Roisnel, T.; Rodríguez-Carvajal, J. WinPLOTR: A Windows Tool for Powder Diffraction Pattern Analysis. *Mater. Sci. Forum* **2001**, *378-381*, 118−123.
(38) Bérar, J.-F.; Lelann, P. E. s.d.'s and Estimated Probable Error Obtained in Rietveld Refinements with Local Correlations. *J. Appl. Crystallogr.* **1991**, *24*, 1−5.
(39) Herklotz, M.; Scheiba, F.; Hinterstein, M.; Nikolowski, K.; Knapp, M.; Dippel, A. C.; Giebeler, L.; Eckert, J.; Ehrenberg, H. Advances in in Situ Powder Diffraction of Battery Materials: A Case Study of the New Beamline P02.1 at DESY, Hamburg. *J. Appl. Crystallogr.* **2013**, *46*, 1117−1127.
(40) Ravel, B.; Newville, M. ATHENA, ARTEMIS, HEPHAESTUS: Data Analysis for X-Ray Absorption Spectroscopy Using IFEFFIT. *J. Synchrotron Radiat.* **2005**, *12*, 537−541.

DOI: 10.1021/acsomega.9b00563
ACS Omega 2019, 4, 9731−9738